Check for updates

Density functional calculations of diffusion paths of CH₃S$_{ad}$ on $c(2 \times 2)$-Cl and -Br covered Cu(100) surfaces†

Falk Wendorff (ID) *[a] and Eckhard Pehlke[ab]

Identification of the atomic-scale mechanisms of surface diffusion at interfaces covered by co-adsorbates is relevant for understanding electrochemical processes at these interfaces. The surface dynamics of CH₃S$_{ad}$ on $c(2 \times 2)$-Cl covered Cu(100) surfaces has been studied with video-STM in electrochemical environment by Yang, Taranowski, and Magnussen [*Langmuir*, 2012, **28**, 14143]. We present density functional calculations to predict diffusion paths and energy barriers of CH₃S$_{ad}$ substitutionally adsorbed on $c(2 \times 2)$-Cl or -Br covered Cu(100) surfaces and compare them to the case of S$_{ad}$. Additional vacancies in the halogen adlayer enable further diffusion paths with significantly lower DFT energy barriers (*i.e.* energy barriers in case of uncharged surfaces *vs.* vacuum). We argue that at least in case of Cl-covered surfaces this preference for vacancy-assisted diffusion of CH₃S$_{ad}$ persists when the energy for creating a Cl-vacancy is accounted for. However, we have not yet been able to include the effect of the electric field on the computed energy barriers for this system, which might affect the preferred diffusion mechanism.

1 Introduction

Given their crucial role in the fields of *e.g.* energy conversion, corrosion, electro-catalysis, and electro-deposition, processes at electrochemical interfaces are investigated intensely.[2–4] In particular, an atomic-scale understanding of the diffusion mechanism of ad-particles at the interfaces is needed.[5] This can be complicated by the presence of a mono-layer of specifically adsorbed (*e.g.* halide) ions from the electrolyte, which are blocking adsorption sites of the diffusing species. Halides are known to affect growth (*e.g.* damascene Cu plating,[6,7] electrochemical annealing[8]) as well as electrocatalytical processes[2,9] at interfaces.

Rahn *et al.*[1] have studied the diffusion of S$_{ad}$ on a Cu(100) surface with a $c(2 \times 2)$ halide coverage. Despite the chemical similarity of Cl and Br, they found distinct differences of S$_{ad}$ tracer atom diffusion between these co-adsorbates. These differences have been traced back to qualitatively different (*i.e.* rotation and exchange) diffusion paths of the sulfur adatom.

Furthermore, the diffusion dynamics of CH₃S$_{ad}$ on $c(2 \times 2)$-Cl covered Cu(100) surfaces has been studied with video-STM by Yang *et al.*[10] Here we present density functional calculations in order to compare diffusion paths of CH₃S$_{ad}$ on Cu(100) surfaces covered by either a $c(2 \times 2)$-Cl or a $c(2 \times 2)$-Br monolayer. A diffusion path similar to the rotation diffusion path by Rahn *et al.* of the sulfur adatom will be examined. In addition, further diffusion paths enabled by the presence of a nearby vacancy in the $c(2 \times 2)$ halogen adlayer will be presented. Results for CH₃S$_{ad}$ will be compared with the diffusion of S$_{ad}$. The probability of vacancies in the halogen layer will be discussed. Our findings emphasize the need to consider vacancy-assisted diffusion and pave the way for future calculations including electrolyte and electric field effects.

2 Computational details

All DFT calculations have been performed with codes from the Quantum ESPRESSO program package, version 6.7.[11–13] The electronic structure has been assumed spin-unpolarized. This has been confirmed by two test calculations allowing for spin-polarization for a configuration with CH₃S$_{ad}$ in the adsorption configuration and at the transition state. In both cases an initial spin polarization at the S-atom disappeared during the electronic relaxation (*i.e.* it is transferred to the unique Fermi

---

[a] *Institut für Theoretische Physik und Astrophysik, Christian-Albrechts-Universität zu Kiel, Olshausenstr. 40, 24098 Kiel, Germany. E-mail: wendorff@physik.uni-kiel.de*

[b] *Kiel Nano, Surface and Interface Science KiNSIS, Kiel University, Germany*

† Electronic supplementary information (ESI) available: (i) A convergence analysis to determine the accuracy of the calculations, (ii) details for the diffusion of CH₃S$_{ad}$ on the Cu(100) surface without coadsorbates, (iii) a comparison to the results of Rahn *et al.*[1] for the rotation path of S$_{ad}$ diffusion and (iv) details on the examined diffusion paths. See DOI: https://doi.org/10.1039/d4cp03884c

This journal is © the Owner Societies 2024

Phys. Chem. Chem. Phys., 2024, **26**, 30035–30043 | **30035**

level of the non-magnetic Cu substrate). The generalized gradient approximation (GGA) for the exchange correlation energy-functional according to Perdew–Burke–Ernzerhof (PBE)[14] has been used. Ultra-soft PBE-GGA pseudopotentials (USPP) have been taken from the databases.[15–17] The surfaces are simulated by a slab geometry with a $p(6 \times 6)$ surface unit cell of the Cu(100) substrate and six Cu layers. The supercell is charge-neutral, *i.e.* any local ionic charges are compensated by a surface image charge density of the metal substrate. Atoms of the bottom two Cu layers are fixed at their bulk positions. The theoretical Cu bulk lattice constant amounts to 3.637 Å, which compares well to other authors.[18–23] The top four substrate layers as well as all adsorbate positions are relaxed. A grid of $4 \times 4 \times 1$ k-points evenly distributed over the first 2D-Brillouin zone of the surface lattice according to Monkhorst and Pack[24] is used. This results in eight inequivalent k-points (only making use of time-reversal symmetry, but disregarding any spacial symmetries). The Fermi surface smearing method according to Methfessel and Paxton is applied.[25] The width of the vacuum between the slabs amounts to at least 16 Å. As the slabs are asymmetric, a dipole correction is applied. The cut-off energy of the plane-waves basis set is set to 35 Ry.

The equilibrium atomic geometries of the initial and final configurations and further energy minimum-configurations along the diffusion paths are found by ionic relaxation, where the residual forces on the ions must be smaller than 10^{-4} Ry a_0^{-1} and the estimated error of the energy due to the electronic convergence must be smaller than 10^{-6} Ry.

To calculate the diffusion paths and the corresponding variations of energy and dipole moment along the paths, the nudged elastic band (NEB) method together with a climbing image (CI) as implemented in PWneb (neb.x) from Quantum ESPRESSO has been used.[26–28] The NEB calculations are assumed to have converged if the force perpendicular to the path on every image is smaller than 0.05 eV Å^{-1} $\approx 2 \times 10^{-3}$ Ry a_0^{-1}. Dipole moments are calculated with the threshold for the electronic convergence set to 10^{-8} Ry. The change in surface dipole moment $\Delta\mu$ is defined as the difference between the component of the electric dipole moment perpendicular to the surface in the transition state and in the initial state. It is related to the induced change in the workfunction of the surface ΔW, $\Delta\mu = -(\varepsilon_0 A/|e|)\Delta W$ where A is the surface area of the periodically repeated supercell and ε_0 the vacuum permittivity.

With these convergence parameters the estimated accuracy of energy differences between a single adsorbate atom at the bridge or hollow site amounts to about ± 0.02 eV and the accuracy of dipole moment differences amounts to about ± 4 me Å with respect to plane-wave energy cutoff, k-point set, width of vacuum and number of substrate layers (for the convergence analysis, see ESI†). Note that in case of S$_{ad}$ and CH$_3$S$_{ad}$ diffusion paths with a larger number of adsorbate atoms dislocated along the diffusion path the uncertainties will be larger than for above simple configurations, the authors of ref. 1 obtain an uncertainty of ± 0.1 eV for the S$_{ad}$ rotation diffusion path. The above estimate does not include any inaccuracy due to the choice of the approximate exchange
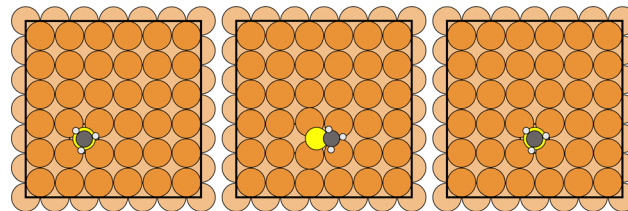

Fig. 1 Atomic configurations (initial, transition and final state) along the diffusion path of CH$_3$S$_{ad}$ on the Cu(100) surface (brown: Cu, yellow: S, black: C, white: H).

correlation-energy functional, which is expected to be larger.‡ [29–32] Moreover, the electrolyte has not been accounted for in our DFT computations.

3 Results

3.1 Diffusion on the Cu(100) surface

CH$_3$S$_{ad}$, either emerging from the dissociation of methanethiol (CH$_3$SH)[33,34] or dimethyl disulfide (CH$_3$SSCH$_3$)[35] deposited on the Cu(100) surface, adsorbs with the sulfur atom in a hollow position of the substrate surface and the S–C bond perpendicular to the surface.[33–35] Similar to the case of S$_{ad}$ on Cu(100),[36] we have investigated the diffusion of the CH$_3$S$_{ad}$ *via* the bridge site of the Cu(100) substrate as shown in Fig. 1.

The energy barrier for CH$_3$S$_{ad}$ is 511 meV. It is less than the energy barrier of 904 meV for S$_{ad}$ (see Fig. 2). Our calculated value is in good agreement with the 881 meV diffusion energy barrier for S$_{ad}$ calculated by Bernard Rodríguez *et al.*,[36] despite the different cell size and the different exchange correlation functional. We suppose that the reduction of the energy barrier can be rationalized in the following way: in case of CH$_3$S$_{ad}$ one of the three p-orbitals of the sulfur atom is bonding to the carbon atom of the methyl group. When the sulfur atom approaches the bridge site, the CH$_3$S$_{ad}$ tilts with respect to the surface normal. Thereby a more favorable bonding configuration between the two p-orbitals perpendicular to the S–C direction and the Cu substrate atoms is achieved.[37] Thus the energy barrier is smaller for a molecule that is tilted than for one artificially kept upright along the diffusion path. At the transition state, on the Cu(100) surface without a halogen adlayer, the S–C bond is tilted by 55° with respect to the surface normal, which is similar to the tilt angle on an unreconstructed Au(111) surface.[37,38] The diffusion energy barrier of CH$_3$S$_{ad}$ is significantly reduced as compared to the diffusion of S$_{ad}$. The additional motion of the methyl group along the diffusion path leads to a distinctly longer path in case of CH$_3$S$_{ad}$ than for S$_{ad}$ (for more information see ESI†). Note that in Fig. 2 the energy is plotted *versus* a scaled reaction coordinate.

3.2 Diffusion in the presence of a $c(2 \times 2)$ halogen adlayer

The diffusion path of CH$_3$S$_{ad}$ on a Cu(100) surface in the presence of a $c(2 \times 2)$ adlayer of halogen coadsorbates has

---

‡ Corresponding calculations are underway.

30036 | *Phys. Chem. Chem. Phys.*, 2024, **26**, 30035–30043
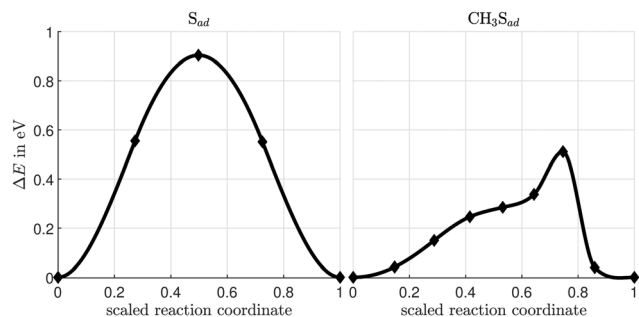
This journal is © the Owner Societies 2024

Fig. 2 Variation of the total energy along the diffusion path for S_{ad} and CH_3S_{ad} on Cu(100).

been constructed starting from the rotation path of S_{ad} diffusing on such a surface proposed by Rahn *et al.*[1] We have reproduced their results (for a comparison see ESI†). Then we have added a methyl group on top of the sulfur. Note that this procedure does not apply to their exchange diffusion path, thus we restrict ourselves to a single CH_3S_{ad} diffusion path on the elsewise completely halogen-covered Cu substrate (Fig. 3).

The energy variation along the rotation diffusion path of S_{ad} and CH_3S_{ad} on the $c(2 \times 2)$-Cl or -Br covered Cu(100) surface is compared in Fig. 4. In the first part of the path the sulfur atom moves to an adjacent hollow site of the substrate lattice. In the remaining (calculated) part of the diffusion path the halogen adatoms rearrange. The collective distortion and rearrangement of the halogens results in a variety of shallow local energy minima with energy barriers between them much smaller than the barrier evoked by the initial hop of the S_{ad}. This is consistent with the known small Cl and Br diffusion energy barrier (Table S2 in ESI†). However, also the repulsion of the adsorbates determines the reaction path. Finally, the complete diffusion path is obtained from the calculated configurations
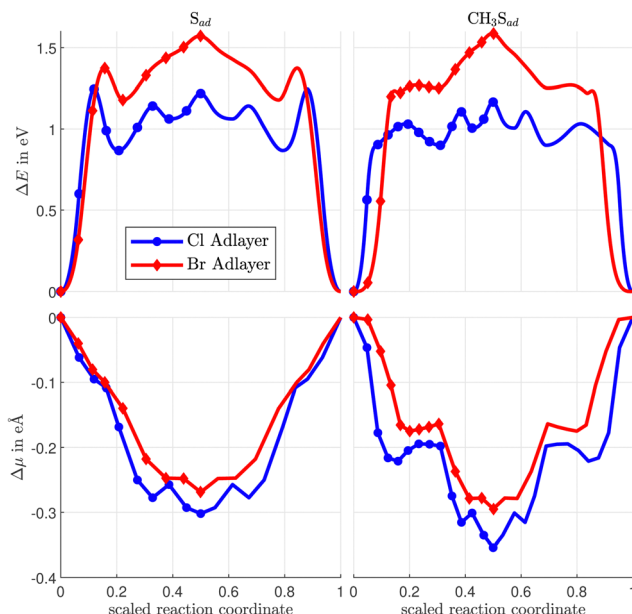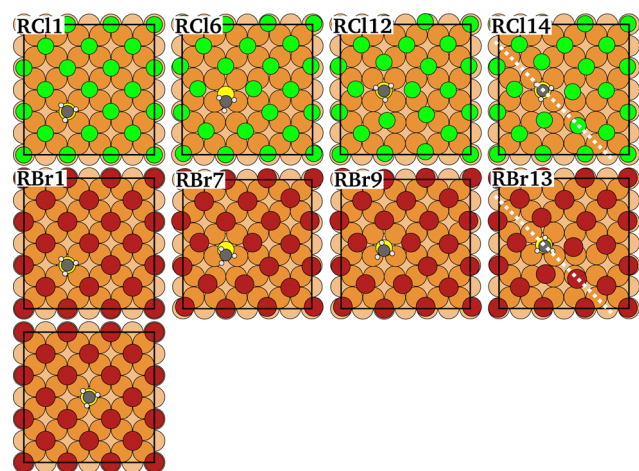

Fig. 3 Atomic configurations along the rotation diffusion path of CH_3S_{ad} on a Cu(100) surface covered by a $c(2 \times 2)$ adlayer of Cl (green) or Br (red). Cl and Br relate to the halogen coverage, the number relates to the number of the image. The dashed line denotes the mirror to obtain the complete diffusion path. The last image shows the final state after the diffusion hop on the Br-covered Cu(100) surface. For details see ESI.†

Fig. 4 Variation of the total energy (top) and the surface dipole moment (bottom) along the diffusion path of S_{ad} and CH_3S_{ad} on the $c(2 \times 2)$-Cl or -Br covered Cu(100) surface.

(solid markers in Fig. 4) by application of a mirror symmetry. (A video showing the energy variation together with the atomic configurations for CH_3S_{ad} for the full path is available in the ESI.†) When the sulfur atom transverses the bridge site the CH_3S_{ad} becomes tilted. Consistent with the observation for diffusion on the clean surface, the corresponding (*i.e.* the first) energy barrier along the diffusion path is smaller in case of CH_3S_{ad} on $c(2 \times 2)$ halogen covered Cu(100) than for S_{ad} on the halogen covered surface. The tilt angle between the S–C bond and the surface normal is slightly smaller than in the case of diffusion without halogen co-adsorbates. In case of the Cl adlayer it amounts to $42°$ and in case of the Br adlayer it is $24°$.

In an electrochemical environment, the activation energy for diffusion is known to depend on the sample potential ϕ.[10,39] For constant (*i.e.* full $c(2 \times 2)$) halide coverage and small potential difference with respect to the potential of zero charge of metal and adsorbate together, the expression by Giesen *et al.*[40] reads

$$E_{act}(\varphi) = E_{act}^{(0)} - \left(\mu^{(TS)} - \mu^{(ads)} \right) \frac{\sigma_0(\varphi)}{\varepsilon_0}, \quad (1)$$

with $E_{act}^{(0)}$ the activation energy at the potential of zero charge ϕ_{pzc}, $\mu^{(TS)}$ the electric dipole moment at the transition state geometry, $\mu^{(ads)}$ the electric dipole moment of the equilibrium configuration of the adsorbate, and $\sigma_0 = C_D(\phi - \phi_{pzc})$ the charge density on the surface. Note that the dipole moments calculated in this work refers to a surface *versus* vacuum, in case of an electrochemical interface the dipole moments may be partially screened by the electrolyte. Experimental estimates for the capacity of the double layer C_D for $c(2 \times 2)$-Cl on Cu(100) are $25 \ \mu F \ cm^{-2}$ (ref. 41) and $16 \ \mu F \ cm^{-2}$ (ref. 42). The "virtual" potential of zero charge of $c(2 \times 2)$-Cl on Cu(100) has been

This journal is © the Owner Societies 2024

Phys. Chem. Chem. Phys., 2024, **26**, 30035–30043 | **30037**

estimated by Schwarz *et al.*[42] to be distinctly more positive than the potential where the Cu surface dissolves (ϕ_{pzc} is more positive than 2.3 V *versus* SHE). Here we do not apply eqn (1) as the difference $\phi - \phi_{pzc}$ is too large. However, we conclude that in the range of sample voltage applied in experiment[10] the activation energy of the CH_3S_{ad} diffusion has to be expected to be smaller than our computed value (which is corresponding to an uncharged surface *vs.* vacuum).

3.3 Diffusion in the presence of a nearest neighbour vacancy in the halogen adlayer

If there is a vacancy in the halogen adlayer nearest neighbour to the S_{ad} or the CH_3S_{ad} further diffusion paths emerge. As the halogens just relax (but do not have to rearrange as they do not occupy different adsorption sites along the diffusion path) the corresponding energy barriers are distinctly smaller than those found in case of the complete $c(2 \times 2)$ halogen layer. In case of S_{ad}, vacancy-assisted diffusion paths have already been calculated by Stremme and Deuchler.[1] In order to compare diffusion activation energies of CH_3S_{ad} to those of S_{ad}, we have re-calculated the S_{ad} diffusion paths using a $p(6 \times 6)$ surface unit cell and the PBE-GGA for the exchange–correlation energy functional. Our results for the diffusion of S_{ad} in Table 1 are fully consistent with their previous data.[1]

We consider two paths (I and II) for the diffusion of S_{ad}, as shown in Fig. 5 and 6. In path I, the S_{ad} diffuses *via* the bridge positions to the vacancy site, while in path II a Cu atom is temporarily pushed out of the surface and the S_{ad} can diffuse through the resulting Cu vacancy.

Three different vacancy assisted diffusion paths for CH_3S_{ad}, A, B, and C are shown in Fig. 7, and the corresponding variation of total energy along the diffusion paths in Fig. 8. The energy expense needed to create the nn-vacancy in the halogen layer will be considered further below.
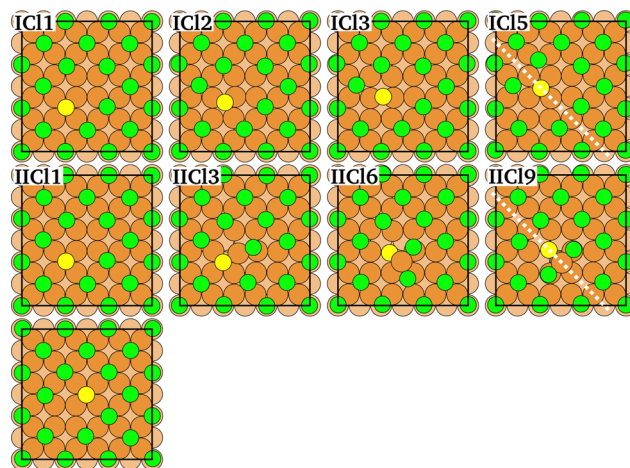

Fig. 5 Atomic configurations along the diffusion paths I and II of S_{ad} on a Cu(100) surface covered by a $c(2 \times 2)$-Cl adlayer with a vacancy in the halogen adlayer. Diffusion paths for the $c(2 \times 2)$-Br adlayer are similar. Such paths have been investigated before.[1] I and II relates to the path. Cl relates to the halogen coverage, the number relates to the number of the image. The dashed line denotes the mirror to obtain the complete diffusion path. The last image shows the final state after the diffusion hop. For details see ESI.†
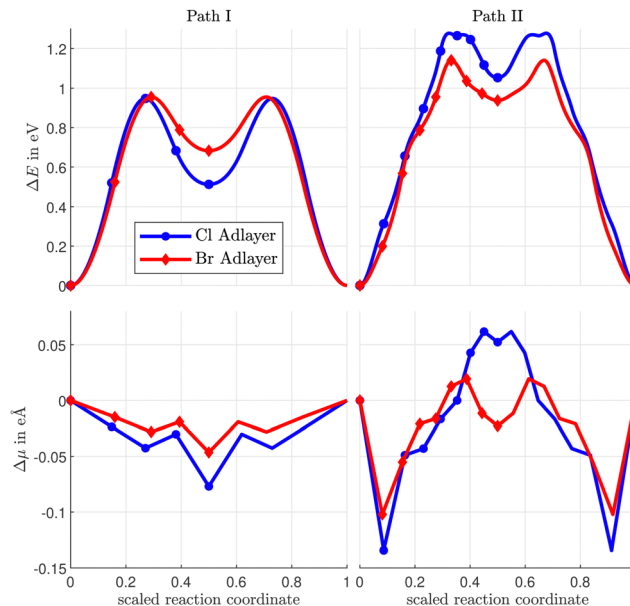

Fig. 6 Variation of the total energy (top) and the electric dipole moment (bottom) along the S_{ad} diffusion paths I and II on a Cu(100) surface with a vacancy in the Cl- or Br-coverage.

Table 1 Changes of the total energy and the surface dipole moment along the S_{ad} and the CH_3S_{ad} diffusion paths on a Cu(100) surface with Cl- or Br-coverage. Data for the S_{ad} exchange path are taken from the literature[1]

Diffusion path	ΔE_{DFT}^{diff} in eV	$\Delta\mu^{TS}$ in e Å
S_{ad} $c(2 \times 2)$-Cl rotation path	1.24	−0.30
S_{ad} $c(2 \times 2)$-Cl exchange path[1]	1.83[1,43]	−0.23[a 1,43]
S_{ad} $c(2 \times 2)$-Br rotation path	1.57	−0.27
S_{ad} $c(2 \times 2)$-Br exchange path[1]	1.48[1,43]	−0.29[a 1,43]
S_{ad} $c(2 \times 2)$-Cl vacancy path I	0.95	−0.04
S_{ad} $c(2 \times 2)$-Cl vacancy path II	1.28	≈0
S_{ad} $c(2 \times 2)$-Br vacancy path I	0.96	−0.03
S_{ad} $c(2 \times 2)$-Br vacancy path II	1.14	0.01
CH_3S_{ad} $c(2 \times 2)$-Cl rotation path	1.17	−0.35
CH_3S_{ad} $c(2 \times 2)$-Br rotation path	1.59	−0.30
CH_3S_{ad} $c(2 \times 2)$-Cl vacancy path A	0.69	−0.11
CH_3S_{ad} $c(2 \times 2)$-Cl vacancy path B	0.83	−0.13
CH_3S_{ad} $c(2 \times 2)$-Cl vacancy path C	0.66	−0.09
CH_3S_{ad} $c(2 \times 2)$-Br vacancy path A	0.81	−0.05
CH_3S_{ad} $c(2 \times 2)$-Br vacancy path B	0.78	−0.09
CH_3S_{ad} $c(2 \times 2)$-Br vacancy path C	0.69	−0.05

[a] Note that a sign change of $\Delta\mu$ can occur along the diffusion path.[1]

Diffusion paths A and C differ in that path A has an additional energy minimum in the middle of the path, where the CH_3S_{ad} is close to neighboring halogens. Path B takes a more direct route between the initial and final states. As a result, path B is shorter than path A and C. The paths also differ in the direction in which the CH_3-group is tilted. While in path A the CH_3-group is tilted in the direction of the diffusion path,
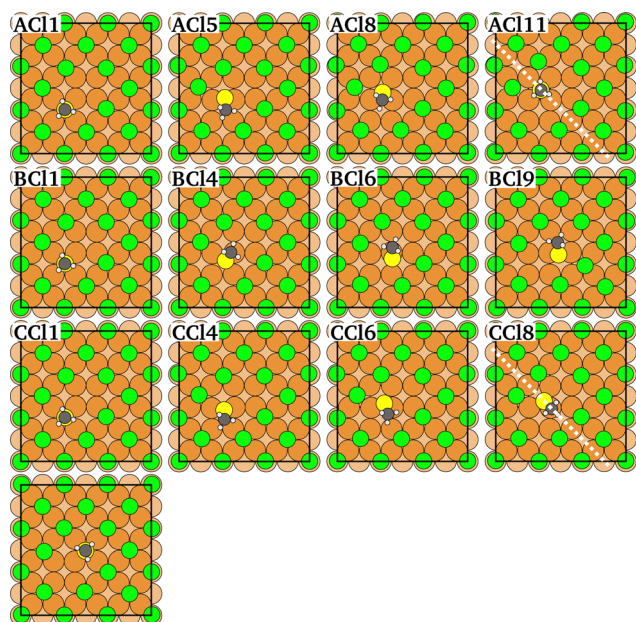
30038 | *Phys. Chem. Chem. Phys.*, 2024, **26**, 30035–30043

This journal is © the Owner Societies 2024

Fig. 7 Atomic configurations along the diffusion paths A, B and C of CH_3S_{ad} on a Cu(100) surface covered by a $c(2 \times 2)$-Cl adlayer with a vacancy in the halogen adlayer. Diffusion paths for the $c(2 \times 2)$-Br adlayer are similar. A, B and C relates to the path. Cl relates to the halogen coverage, the number relates to the number of the image. The dashed line denotes the mirror to obtain the complete diffusion path. The last image shows the final state after the diffusion hop. For details see ESI.†

the tilting in path B and path C is partially at an angle to the diffusion path. (Videos of the diffusion paths can be found in the ESI.†)

The diffusion energy barriers (*i.e.* the maximum of the total energy increase ΔE_{DFT}^{diff} along the diffusion paths) and the corresponding induced electric dipole moments

$\Delta\mu^{TS} = \mu^{(TS)} - \mu^{(ads)}$ are summarized in Table 1. In case of CH_3S_{ad} the diffusion paths A, B and C for the vacancy-assisted diffusion have significantly lower energy barriers than the rotation diffusion path. Among all considered calculated paths A, B, and C, in case of both halogen adlayers the diffusion path C turns out to be the most favorable one. However, vacancy assisted diffusion paths with energy barriers within some tens of meV can all contribute simultaneously to diffusion, and, moreover, are not distinguishable within the accuracy of DFT calculations, in particular in view of the approximate XC energy functionals. For all CH_3S_{ad} diffusion paths the variation of the electric dipole moment $\Delta\mu^{TS}$ is negative. This is consistent with the displacement in the z-direction (*i.e.* perpendicular to the surface) of the negatively charged sulfur and halogen ad-atoms along the diffusion path. The effect is larger in case of the rotation path, due to the large outward displacements of the halogens in the z-direction. The z-coordinates of the halogens change less during diffusion of CH_3S_{ad} in the presence of a nearest neighbour halogen vacancy (see ESI†). $\Delta\mu^{TS}$ is slightly positive in case of path II for the Br coadsorbate showing an inward motion of the diffusing S_{ad}, in agreement with previous calculations.[1]

The energy barriers in the rotation paths differ only slightly between S_{ad} and CH_3S_{ad}, since the CH_3-group is not tilted in the transition state (1.24 eV *vs.* 1.17 eV for Cl and 1.57 eV *vs.* 1.59 eV for Br). The situation is different for the energy barriers of the vacancy paths over the bridge position. Since the CH_3-group is tilted in the transition state, the energy barrier for CH_3S_{ad} is lower than for S_{ad}. This is consistent with the results from the clean Cu(100) surface. As pointed out above, there is no analogue to the S_{ad} exchange diffusion path on the $c(2 \times 2)$ halogen-covered surface in case of CH_3S_{ad} due to geometrical constraints.

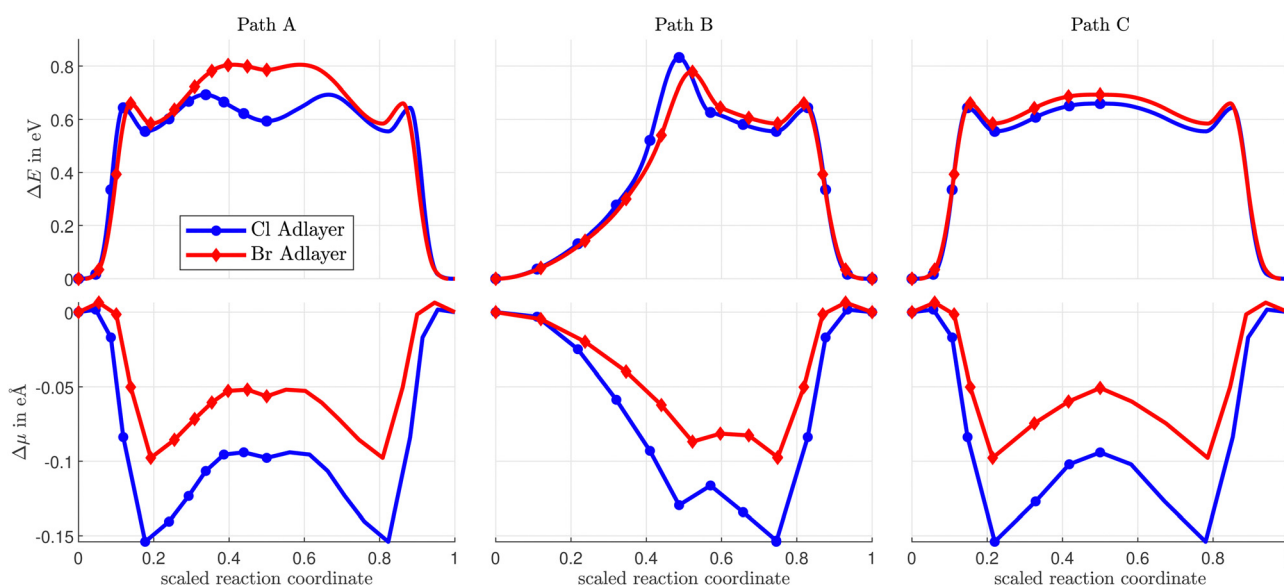**Fig. 8** Variation of the total energy (top) and the electric dipole moment (bottom) along the CH_3S_{ad} diffusion paths A, B and C on a Cu(100) surface with a vacancy in the Cl- or Br-coverage.

This journal is © the Owner Societies 2024

Phys. Chem. Chem. Phys., 2024, **26**, 30035–30043 | **30039**

3.4 Estimate of the frequency of halogen vacancies and its effect on vacancy-assisted diffusion

To obtain a rough estimate for the vacancy-assisted hopping rate of the CH_3S_{ad} on the halogen-covered Cu(100) surface we start from the expression

$$\nu_{hop} = \kappa \nu_0 e^{-\beta E^{diff}(\phi)} \qquad (2)$$

for the hopping rate over an energy barrier E^{diff} from transition state theory.[44,45] In case of vacancy-assisted hopping this gives the conditional hopping rate, provided that there already exists a nn vacancy in the halogen layer. The prefactor ν_0 denotes an attempt frequency, which has not been calculated here. It is assumed to be of the order of 10^{12} Hz. The attempt frequency for S_{ad} diffusing on a Cl-covered Cu(100) surface is of similar order of magnitude, $(2.35 \pm 0.35) \times 10^{12}$ Hz.[39] The inverse of temperature is denoted as $\beta = 1/k_B T$. $E^{diff}(\phi)$ is the activation energy barrier of the diffusion hop (A, B, or C), which in electrochemical environment additionally depends on the sample potential ϕ. The diffusion energy barriers at the potential of zero charge are taken to be approximately equal to ΔE_{DFT}^{diff} in Table 1. Here, any additional local energy minima (that indicate local equilibrium configurations along the diffusion path) are disregarded. Just the maximum of the energy along the reaction path is considered to obtain ΔE_{DFT}^{diff}, thus ignoring recrossings[46] of the transition state by the diffusing species. These can be accounted for by an appropriate transmission factor κ. Alternatively, if the intermediate energy barriers are sufficiently large compared to a few times the thermal energy, a Master equation could be solved,[47] but this is beyond the scope of our estimate. As the diffusion of the CH_3S_{ad} is supported by a neighboring vacancy in the halogen adlayer, the probability p_{vac} for the occurrence of such a nearest neighbour vacancy has to be considered. As the hopping rates of the halogens are much larger than the hopping rate of the CH_3S_{ad}[48] (here we assume a similar prefactor for both, as well as no huge increase of the hopping energy barrier of the halogen vacancy when it comes close to the CH_3S_{ad}) any correlation between the direction of consecutive hops of the CH_3S_{ad} is neglected.[49] The hopping rate is thus approximated as

$$\nu = p_{vac} \kappa \nu_0 e^{-\beta E^{diff}(\phi)}. \qquad (3)$$

To estimate the probability of a halogen vacancy in the $c(2 \times 2)$ halogen adlayer (without any co-adsorbed CH_3S_{ad}) as a function of sample potential in an electrochemical environment we follow the approach of Mitchell et al.,[50,51] who applied an Ising-type lattice gas Hamiltonian,

$$H(\{c_i\}) - \bar{\mu} N_{ads} = \frac{1}{2} \sum_{i \neq j=1}^{L^2} J_{ij} c_i c_j - \bar{\mu} \sum_{i=1}^{L^2} c_i, \qquad (4)$$

to compute the chemisorption isotherm of Br^- on Ag(100). The sum extends over all L^2 hollow sites of the $p(1 \times 1)$ substrate lattice. $c_i \in \{0,1\}$ is the halogen occupation number of the i-th site, $N_{ads} = \sum_{i=1}^{L^2} c_i$ the number of adsorbates, J_{ij} the adatom interaction between sites i and j, and

$$\bar{\mu} = \bar{\mu}_0 + k_B T \ln \frac{c}{c_0} - e\gamma(\varphi - \varphi_{ref}) \qquad (5)$$

with T denoting the temperature, $c = [Br^-]$ the Br^- concentration, c_0 a reference concentration, e the (positive) elementary charge, γ the (negative) electrosorption valency of the halide ion, $\phi - \phi_{ref}$ the electric potential with respect to a reference electrode, and $\bar{\mu}_0$ an energy reference.[50] For above model Hamiltonian, with increasing potential there occurs a phase transition from a disordered (1×1) halide adlayer into a $c(2 \times 2)$ reconstructed adlayer.[50] If the sample voltage where the order–disorder transition occurs is known from experiment, this can be used to adjust the $\mu(\phi)$-scale in eqn (5) to the sample voltage scale used in experiment. We shall make use of this procedure in case of the Cl-adlayer on Cu(100) further below.

The Hamiltonian (4) can be re-formulated in terms of vacancies in the nearly complete $c(2 \times 2)$ adlayer. To this purpose the c_i are set equal to zero for all sites of the unoccupied sublattice, and $c_i = 1 - \sigma_i$, for all i running over the sites of the halide $c(2 \times 2)$ sublattice. Finally, interactions between different vacancies are neglected. This conforms to a Langmuir adsorption isotherm model applied to a low coverage of approximately non-interacting halide vacancies. The probability $p_{vac}^{(0)}$ to observe a vacancy at a particular site (e.g. the $i = 1$ site) in the $c(2 \times 2)$ sublattice in this case becomes

$$p_{vac}^{(0)} \approx \exp\left[-\beta\left(\bar{\mu} - \sum_{j=2}^{L^2/2} J_{1j}\right)\right]. \qquad (6)$$

The sum describes the interaction of a single halide at a particular site, here site no. 1, with all other remaining $L^2/2 - 1$ halides of the complete $c(2 \times 2)$ adlayer. Eqn (6) corresponds to a lattice gas of non-interacting halogen vacancies in the $c(2 \times 2)$ adsorbate superlattice with a renormalized adsorption energy of the halogen. The next step is to transport the halogen vacancy to the required position nearest neighbour to the CH_3S_{ad}. The energy difference is denoted $\Delta E_{nn}^{vac}(\phi)$. Values from our DFT calculations are summarized in Table 2. In view of the very small differences of the electric dipole moment of the vacancy close to, and far away from the CH_3S_{ad} (denoted $\Delta\mu^{vac}$ in Table 2) the dependence of ΔE_{nn}^{vac} on the sample potential is neglected. The probability p_{vac} thus becomes

$$p_{vac} = p_{vac}^{(0)} e^{-\beta \Delta E_{nn}^{vac}}. \qquad (7)$$

Inserting this expression, together with $p_{vac}^{(0)}$ from eqn (6), into

Table 2 Difference of the total energy and of the surface dipole moment for a halogen vacancy nearest neighbor to, or far from, the S_{ad} or CH_3S_{ad}

Adsorbate	$\Delta E_{nn,DFT}^{vac}$ in meV	$\Delta\mu^{vac}$ in me Å
$S_{ad}/c(2 \times 2)$-Cl	−2	23
$S_{ad}/c(2 \times 2)$-Br	26	16
$CH_3S_{ad}/c(2 \times 2)$-Cl	10	12
$CH_3S_{ad}/c(2 \times 2)$-Br	33	5

30040 | *Phys. Chem. Chem. Phys.*, 2024, **26**, 30035–30043

This journal is © the Owner Societies 2024

the hopping rate from eqn (3) yields

$$\nu \approx \kappa \nu_0 \exp\left[-\beta\left(E^{\text{diff}}(\varphi) + \Delta E^{\text{vac}}_{\text{nn}} + \bar{\mu} - \sum_{j=2}^{L^2/2} J_{1j}\right)\right]. \quad (8)$$

In experiment, an effective activation energy of the diffusion process is derived by assuming an exponential relation between the hopping rate and $-\beta$ times the effective activation energy. Then the activation energy can be plotted *versus* the sample potential ϕ.[10] Using eqn (5) and (8) and neglecting any ϕ-dependence of the transmission factor κ, the slope of this curve is determined by the derivative of the energy in the exponent in eqn (8) with respect to the sample potential ϕ,

$$\frac{\partial E^{\text{diff}}(\varphi)}{\partial \varphi} - e\gamma. \quad (9)$$

For Cl and Br on Ag(111), Hörmann *et al.*[52] report a calculated electrosorption valency in the range −0.8 to −0.4. This fits with other values for the electrosorption valency of halogens on metal surfaces§ and the assessment that $|\gamma_{\text{Cl}}| < 1$ on the Cu(100) surface.[64] In view of the negative dipole moment change along the diffusion path, which is pointing to a shift of negative charge density in the direction away from the bulk along the diffusion path, $\dfrac{\partial E^{\text{diff}}(\varphi)}{\partial \varphi}$ is expected to be positive.

Next we connect the zero of our halogen chemical potential scale with the sample potential as measured in experiment by using the order–disorder transition as a reference point. In the following we focus solely on the case of the Cl⁻ adlayer on Cu(100). In surface X-ray diffraction experiments of Cl⁻-adsorption on Cu(100) the $c(2 \times 2)$ superstructure intensity is observed at sample potential more positive than ≈ -0.62 $V_{\text{Ag/AgCl}}$ and the Cl⁻ adsorption/desorption with remaining $c(2 \times 2)$ superstructure is detected over a range of about 0.3 V before it saturates.[65] As pointed out by Mitchell *et al.*, in their Monte Carlo simulations the (1×1) to $c(2 \times 2)$ transition occurs at a halogen coverage similar to the critical coverage of the respective hard square model, $\Theta_{\text{crit}} = 0.368$.[51,66] We roughly approximate the Cl coverage of the Cu(100) surface (at high coverage) by a Frumkin isotherm with adsorption sites restricted to a single $c(2 \times 2)$ sublattice of adsorption sites and the Cl–Cl interaction energy parameter $b = \sum\limits_{j=1}^{L^2} J_{1j} \approx 357$ meV. The interaction energy b has been derived from the difference of the DFT adsorption energies of a Cl atom on either the clean ($E^{\text{Cl}}_{\text{ads}}(\text{Cu}(100))$) or the elsewise fully $c(2 \times 2)$-Cl covered Cu(100) surface ($E^{\text{Cl}}_{\text{ads}}(c(2 \times 2)\text{Cl}/\text{Cu}(100))$),

$$b = E^{\text{Cl}}_{\text{ads}}(c(2 \times 2)\text{Cl}/\text{Cu}(100)) - E^{\text{Cl}}_{\text{ads}}(\text{Cu}(100)). \quad (10)$$

It means that the Cl⁻ adsorption isotherm has a considerable spread on the potential axis due to adsorbate interactions. The critical chemical potential of the order–disorder transition is approximated by the value of the chemical potential where the coverage of the Frumkin isotherm equals the critical coverage $\Theta_{\text{crit}} = 0.368$. Assuming $c = c_0$ in eqn (5) we obtain

$$\bar{\mu} = 0.29 \text{ [eV]} - e\gamma(\phi_{\text{Ag/AgCl}} + 0.62 \text{ [V]}). \quad (11)$$

In the STM experiment by Yang *et al.*[10] diffusion rates of the $\text{CH}_3\text{S}_{\text{ad}}$ have been measured for a range of sample potentials from −0.4 V_{SCE} up to −0.25 V_{SCE}. Taking the extreme value $\gamma = -1$ for the electrosorption valency, in this range of sample potential the contribution from the vacancy abundancy to the activation energy ($\Delta E^{\text{vac}}_{\text{nn,DFT}} + \bar{\mu} - 0.357$ [eV], which is added to the barrier height $E_{\text{diff}}(\phi)$) stays below 0.36 eV. Thus, as long as the effect of the electric field on the diffusion energy barriers is ignored, the vacancy assisted diffusion path of $\text{CH}_3\text{S}_{\text{ad}}$ on $c(2 \times 2)$-Cl/Cu(100) is preferred by at least 0.15 eV. However, as the electric dipole moment change along the diffusion path is distinctly more negative for the rotation path than for the vacancy-assisted diffusion path (see Table 1) we cannot exclude that a strong negative charge density on the sample surface might lead to a preference for the rotation path. At present we cannot quantify the electric field effect due to reasons explained above.

4 Conclusions

In this paper we have presented DFT-calculations for various diffusion paths of $\text{CH}_3\text{S}_{\text{ad}}$ on $c(2 \times 2)$-Cl or -Br covered Cu(100) surfaces and compare to the case of S_{ad} diffusion on these surfaces. For $\text{CH}_3\text{S}_{\text{ad}}$ substitutionally adsorbed in an elsewise complete $c(2 \times 2)$ overlayer of the halogen, we have generalized the rotation diffusion path by Rahn *et al.*[1] for S_{ad}. The DFT diffusion energy barrier (*i.e.* the diffusion energy barrier on an adsorbate-covered surface *versus* vacuum) for $\text{CH}_3\text{S}_{\text{ad}}$ is 1.17 eV in case of the Cl-coadsorbate and 1.59 eV in case of Br. Furthermore, we have found diffusion paths assisted by vacancies in the halogen layer with considerably lower DFT diffusion energy barriers. For $\text{CH}_3\text{S}_{\text{ad}}$, in case of the Cl-coadsorbate the vacancy lowers the DFT energy barrier of the diffusion hop by 0.51 eV to a value of 0.66 eV and, in case of the Br-coadsorbate, by 0.89 eV to 0.69 eV. For S_{ad} the reduction in the energy barrier is smaller, it amounts to 0.29 eV in case of the Cl adlayer and 0.52 eV in case of the Br adlayer.

Within the range of Cl chemical potential covered by the video STM data by Yang *et al.*[10] the energy expense to create vacancies in the $c(2 \times 2)$ adlayer is small enough so that, as long as variation of the energy barrier heights due to electric field effects are ignored, a vacancy-assisted diffusion path of the $\text{CH}_3\text{S}_{\text{ad}}$ is preferred. However, including the variation of the energy barriers as a function of sample potential could alter this.

Experimentally, Yang *et al.* have reported a linear potential dependence of +0.5 eV V⁻¹ for the diffusion barrier of $\text{CH}_3\text{S}_{\text{ad}}$

§ $\gamma_{\text{Cl}} = -0.7 \pm 0.3$ on Au(100);[53] $\gamma_{\text{Cl}} = -0.5 \pm 0.3$ on Au(111);[54] $\gamma_{\text{Br}} = -0.76$ on Au(111);[55] $\gamma_{\text{Br}} = -0.63$ on Au(100);[55] $\gamma_{\text{Br}} = -0.4$ on Au(110);[55] $\gamma_{\text{Br}} = -0.7$ on Au(311);[55] $\gamma_{\text{Br}} = -0.54 \pm 0.05$ on Au;[56] $\gamma_{\text{Br}} = -0.7 \pm 0.15$ on Ag(100);[57] $\gamma_{\text{Br}} = -0.75 \pm 0.5$ on Au(100);[58] $\gamma_{\text{Cl}} = -0.5 \pm 0.2$ on Au(111);[59] $\gamma_{\text{Br}} = -0.7 \pm 0.2$ on Au(111);[59] $\gamma_{\text{Br}} = -0.99$ on Pt(100);[60] $\gamma_{\text{Br}} = -0.99$ on Pt(111);[61] $\gamma_{\text{Cl}} = -1.0 \pm 0.2$ on Au(111);[62] $\gamma_{\text{Cl}} = -1$ on Pt(111);[63] $\gamma_{\text{Br}} = -0.73 \pm 0.03$ on Ag(100).[50]

This journal is © the Owner Societies 2024

Phys. Chem. Chem. Phys., 2024, **26**, 30035–30043 | **30041**

on a Cu(100) surface with a $c(2 \times 2)$-Cl adlayer.[10] The sign of the slope is compatible with both diffusion mechanisms, the rotation diffusion path and the vacancy-assisted diffusion. Future calculations taking care of the electrochemical environment are thus desirable, which include the electrolyte and quantify the variation of the diffusion energy barriers $E_{\mathrm{diff}}(\phi)$ with the sample potential ϕ.

Author contributions

Supervision by EP, DFT calculations and visualizations by FW, writing of manuscript by FW and EP.

Data availability

The data that support the findings of this study are available from the corresponding author upon reasonable request.

Conflicts of interest

There are no conflicts to declare.

Notes and references

1 B. Rahn, R. Wen, L. Deuchler, J. Stremme, A. Franke, E. Pehlke and O. M. Magnussen, *Angew. Chem., Int. Ed.*, 2018, **57**, 6065–6068.

2 A. S. Varela, W. Ju, T. Reier and P. Strasser, *ACS Catal.*, 2016, **6**, 2136–2144.

3 O. M. Magnussen, *Chem. – Eur. J.*, 2019, **25**, 12865.

4 O. M. Magnussen and A. Groß, *J. Am. Chem. Soc.*, 2019, **141**, 4777.

5 A.-K. Henẞ, S. Sakong, P. K. Messer, J. Wiechers, R. Schuster, D. C. Lamb, A. Groß and J. Wintterlin, *Science*, 2019, **363**, 715.

6 T. P. Moffat, D. Wheeler and D. Josell, *J. Electrochem. Soc.*, 2004, **151**, C262.

7 P. M. Vereecken, R. A. Binstead, H. Deligianni and P. C. Andricacos, *IBM J. Res. Dev.*, 2005, **49**, 3–18.

8 E. Pichardo-Pedrero, G. L. Beltramo and M. Giesen, *Appl. Phys. A: Mater. Sci. Process.*, 2007, **87**, 461.

9 J. J. Masana, B. Peng, Z. Shuai, M. Qiu and Y. Yu, *J. Mater. Chem. A*, 2022, **10**, 1086–1104.

10 Y.-C. Yang, A. Taranovskyy and O. M. Magnussen, *Langmuir*, 2012, **28**, 14143–14154.

11 P. Giannozzi, S. Baroni, N. Bonini, M. Calandra, R. Car, C. Cavazzoni, D. Ceresoli, G. L. Chiarotti, M. Cococcioni, I. Dabo, A. Dal Corso, S. de Gironcoli, S. Fabris, G. Fratesi, R. Gebauer, U. Gerstmann, C. Gougoussis, A. Kokalj, M. Lazzeri, L. Martin-Samos, N. Marzari, F. Mauri, R. Mazzarello, S. Paolini, A. Pasquarello, L. Paulatto, C. Sbraccia, S. Scandolo, G. Sclauzero, A. P. Seitsonen, A. Smogunov, P. Umari and R. M. Wentzcovitch, *J. Phys.: Condens. Matter*, 2009, **21**, 395502.

12 P. Giannozzi, O. Andreussi, T. Brumme, O. Bunau, M. B. Nardelli, M. Calandra, R. Car, C. Cavazzoni, D. Ceresoli, M. Cococcioni, N. Colonna, I. Carnimeo, A. D. Corso, S. de Gironcoli, P. Delugas, R. A. DiStasio, A. Ferretti, A. Floris, G. Fratesi, G. Fugallo, R. Gebauer, U. Gerstmann, F. Giustino, T. Gorni, J. Jia, M. Kawamura, H.-Y. Ko, A. Kokalj, E. Küçükbenli, M. Lazzeri, M. Marsili, N. Marzari, F. Mauri, N. L. Nguyen, H.-V. Nguyen, A. O. de-la Roza, L. Paulatto, S. Poncé, D. Rocca, R. Sabatini, B. Santra, M. Schlipf, A. P. Seitsonen, A. Smogunov, I. Timrov, T. Thonhauser, P. Umari, N. Vast, X. Wu and S. Baroni, *J. Phys.: Condens. Matter*, 2017, **29**, 465901.

13 Quantum Espresso Foundation, *Quantum Espresso v. 6.7*, 2020, https://gitlab.com/QEF/q-e/-/releases/qe-6.7MaX-Release, accessed on May 24, 2021.

14 J. P. Perdew, K. Burke and M. Ernzerhof, *Phys. Rev. Lett.*, 1996, **77**, 3865–3868.

15 K. F. Garrity, J. W. Bennett, K. M. Rabe and D. Vanderbilt, *Comput. Mater. Sci.*, 2014, **81**, 446–452.

16 A. Dal Corso, *Comput. Mater. Sci.*, 2014, **95**, 337–350.

17 Quantum Espresso Foundation, *Original QE PP library*, 2008, https://pseudopotentials.quantum-espresso.org/legacy_tables/original-qe-pp-library, accessed on March 1, 2022.

18 K. Lejaeghere, V. V. Speybroeck, G. V. Oost and S. Cottenier, *Crit. Rev. Solid State Mater. Sci.*, 2014, **39**, 1–24.

19 P. Janthon, S. M. Kozlov, F. Viñes, J. Limtrakul and F. Illas, *J. Chem. Theory Comput.*, 2013, **9**, 1631–1640.

20 M. Harrison, D. Woodruff and J. Robinson, *Surf. Sci.*, 2008, **602**, 226–234.

21 S. Chen, S. Sun, B. Lian, Y. Ma, Y. Yan and S. Hu, *Surf. Sci.*, 2014, **620**, 51–58.

22 J. P. Perdew, S. Kurth, A. Zupan and P. Blaha, *Phys. Rev. Lett.*, 1999, **82**, 2544–2547.

23 A. Migani and F. Illas, *J. Phys. Chem. B*, 2006, **110**, 11894–11906.

24 H. J. Monkhorst and J. D. Pack, *Phys. Rev. B: Condens. Matter Mater. Phys.*, 1976, **13**, 5188–5192.

25 M. Methfessel and A. T. Paxton, *Phys. Rev. B: Condens. Matter Mater. Phys.*, 1989, **40**, 3616–3621.

26 G. Mills, H. Jónsson and G. K. Schenter, *Surf. Sci.*, 1995, **324**, 305–337.

27 D. Sheppard, R. Terrell and G. Henkelman, *J. Chem. Phys.*, 2008, **128**, 134106.

28 G. Henkelman, B. P. Uberuaga and H. Jónsson, *J. Chem. Phys.*, 2000, **113**, 9901–9904.

30042 | *Phys. Chem. Chem. Phys.*, 2024, **26**, 30035–30043

This journal is © the Owner Societies 2024

29 J. J. Mortensen, K. Kaasbjerg, S. L. Frederiksen, J. K. Nørskov, J. P. Sethna and K. W. Jacobsen, *Phys. Rev. Lett.*, 2005, **95**, 216401.

30 K. Yang, J. Zheng, Y. Zhao and D. G. Truhlar, *J. Chem. Phys.*, 2010, **132**, 164117.

31 Z. Wei, F. Göltl and P. Sautet, *J. Chem. Theory Comput.*, 2021, **17**, 7862–7872.

32 M. Schwarzer, N. Hertl, F. Nitz, D. Borodin, J. Fingerhut, T. N. Kitsopoulos and A. M. Wodtke, *J. Phys. Chem. C*, 2022, **126**, 14500–14508.

33 A. Imanishi, S. Takenaka, T. Yokoyama, Y. Kitajima and T. Ohta, *J. Phys. IV*, 1997, **7**, C2-701–C2-702.

34 M. S. Kariapper, C. Fisher, D. P. Woodruff, B. C. C. Cowie and R. G. Jones, *J. Phys.: Condens. Matter*, 2000, **12**, 2153–2161.

35 F. Bussolotti, M. G. Betti and C. Mariani, *Phys. Rev. B: Condens. Matter Mater. Phys.*, 2006, **74**, 125422.

36 C. R. Bernard Rodríguez and J. A. Santana, *J. Chem. Phys.*, 2018, **149**, 204701.

37 A. Franke and E. Pehlke, *Phys. Rev. B: Condens. Matter Mater. Phys.*, 2010, **81**, 075409.

38 A. Franke and E. Pehlke, *Phys. Rev. B: Condens. Matter Mater. Phys.*, 2009, **79**, 235441.

39 T. Tansel and O. M. Magnussen, *Phys. Rev. Lett.*, 2006, **96**, 026101.

40 M. Giesen, G. Beltramo, S. Dieluweit, J. Müller, H. Ibach and W. Schmickler, *Surf. Sci.*, 2005, **595**, 127–137.

41 M. Vogt, A. Lachenwitzer, O. Magnussen and R. Behm, *Surf. Sci.*, 1998, **399**, 49–69.

42 K. Schwarz, M. C. Groenenboom, T. P. Moffat, R. Sundararaman and J. Vinson, *J. Phys. Chem. Lett.*, 2021, **12**, 440–446.

43 L. Deuchler, private communication.

44 G. H. Vineyard, *J. Phys. Chem. Solids*, 1957, **3**, 121–127.

45 H. O. Pritchard, *J. Phys. Chem. A*, 2005, **109**, 1400–1404.

46 D. G. Truhlar, B. C. Garrett and S. J. Klippenstein, *J. Phys. Chem.*, 1996, **100**, 12771–12800.

47 A. Franke and E. Pehlke, *Phys. Rev. B: Condens. Matter Mater. Phys.*, 2010, **82**, 205423.

48 S. Kenny, J. Pethica and R. Edgell, *Surf. Sci.*, 2003, **524**, 141–147.

49 A. D. Leclaire and A. B. Lidiard, *Philos. Mag.*, 1956, **1**, 518–527.

50 S. Mitchell, G. Brown and P. Rikvold, *J. Electroanal. Chem.*, 2000, **493**, 68–74.

51 S. Mitchell, G. Brown and P. Rikvold, *Surf. Sci.*, 2001, **471**, 125–142.

52 N. G. Hörmann, N. Marzari and K. Reuter, *npj Comput. Mater.*, 2020, **6**, 136.

53 M. Ávila, M. F. Juárez and E. Santos, *ChemElectroChem*, 2020, **7**, 4269–4282.

54 Z. Shi and J. Lipkowski, *J. Electroanal. Chem.*, 1996, **403**, 225–239.

55 C. Nguyen Van Huong, C. Hinnen and A. Rousseau, *J. Electroanal. Chem. Interfacial Electrochem.*, 1983, **151**, 149–162.

56 R. Adzić, E. Yeager and B. Cahan, *J. Electroanal. Chem. Interfacial Electrochem.*, 1977, **85**, 267–276.

57 T. Wandlowski, J. Wang and B. Ocko, *J. Electroanal. Chem.*, 2001, **500**, 418–434.

58 Z. Shi, J. Lipkowski, S. Mirwald and B. Pettinger, *J. Chem. Soc., Faraday Trans.*, 1996, **92**, 3737–3746.

59 J. Lipkowski, Z. Shi, A. Chen, B. Pettinger and C. Bilger, *Electrochim. Acta*, 1998, **43**, 2875–2888.

60 N. M. Marković, C. A. Lucas, H. A. Gasteiger and P. N. Ross, *Surf. Sci.*, 1996, **365**, 229–240.

61 H. A. Gasteiger, N. M. Marković and P. N. Ross, *Langmuir*, 1996, **12**, 1414–1418.

62 O. M. Magnussen, B. M. Ocko, R. R. Adzic and J. X. Wang, *Phys. Rev. B: Condens. Matter Mater. Phys.*, 1995, **51**, 5510–5513.

63 R. Gomez, J. M. Feliu and H. D. Abruna, *J. Phys. Chem.*, 1994, **98**, 5514–5521.

64 G. M. Brisard, E. Zenati, H. A. Gasteiger, N. M. Marković and P. N. Ross, *Langmuir*, 1997, **13**, 2390–2397.

65 Y. Gründer, D. Kaminski, F. Golks, K. Krug, J. Stettner, O. M. Magnussen, A. Franke, J. Stremme and E. Pehlke, *Phys. Rev. B: Condens. Matter Mater. Phys.*, 2010, **81**, 174114.

66 F. H. Ree and D. A. Chesnut, *J. Chem. Phys.*, 1966, **45**, 3983.

This journal is © the Owner Societies 2024

Phys. Chem. Chem. Phys., 2024, **26**, 30035–30043 | **30043**